Low-Power MIMO Signal Processing

Lei Wang, *Member, IEEE,* and Naresh R. Shanbhag, *Senior Member, IEEE*

Abstract—In this paper, we present a new adaptive error-cancellation (AEC) technique, denoted as multi-input–multi-output (MIMO)-AEC, for the design of low-power MIMO signal processing systems. The MIMO-AEC technique builds on the previously proposed AEC technique by employing an algorithm transformation denoted as MIMO decorrelating (MIMO-DECOR) transform. MIMO-DECOR reduces complexity by exploiting correlations inherent in MIMO systems, thereby improving the energy efficiency of AEC. The proposed MIMO-AEC enables energy minimization of MIMO systems by correcting transient/soft errors that arise in very large scale integration signal processing implementations due to inherent process nonidealities and/or aggressive low-power design styles, such as voltage overscaling. We employ the MIMO-AEC in the design of a low-power Gigabit Ethernet 1000Base-T device. Simulation results indicate 69.1%–64.2% energy savings over optimally voltage-scaled present-day systems with no loss in algorithmic performance.

Index Terms—Adaptive filtering, algorithm transformations, algorithmic noise-tolerance, digital filter, Gigabit Ethernet, low power, multi-input–multi-output (MIMO) signal processing, voltage scaling.

I. INTRODUCTION

POWER reduction is essential for high-performance signal processing and communication systems such as Gigabit Ethernet [1], [2], next generation digital subscriber loop (DSL) [3], [4], and future third generation (3G) wireless [5], [6]. Numerous low-power techniques developed so far combined with the benefits of technology scaling have led to the proliferation of high-throughput computing and communication systems with increasingly higher functionality [7]–[10]. With feature sizes being reduced into the deep submicron (DSM) regime, the emergence of DSM noise [11], [12] (due to physical phenomena such as ground bounce [13], [14], crosstalk [15], [16], leakage [17], process variations [18], etc.) as well as increasingly stringent requirements on power/performance have raised concerns about our ability to maintain reliability in an affordable manner in future CMOS technologies. This demands a new design paradigm where reliability and energy-efficiency are addressed in a cohesive manner.

While low-power techniques have been proposed at all levels of very large scale integration (VLSI) design abstraction [7]–[10], very little work has been done in developing power

L. Wang is with the Microprocessor Technology Laboratories, Hewlett Packard Company, Fort Collins, CO 80521 USA (e-mail: lei.wang@onebox.com).

N. R. Shanbhag is with the Coordinated Science Laboratory, Department of Electrical and Computer Engineering, University of Illinois at Urbana-Champaign, Urbana, IL 61801 USA (e-mail: shanbhag@uiuc.edu).
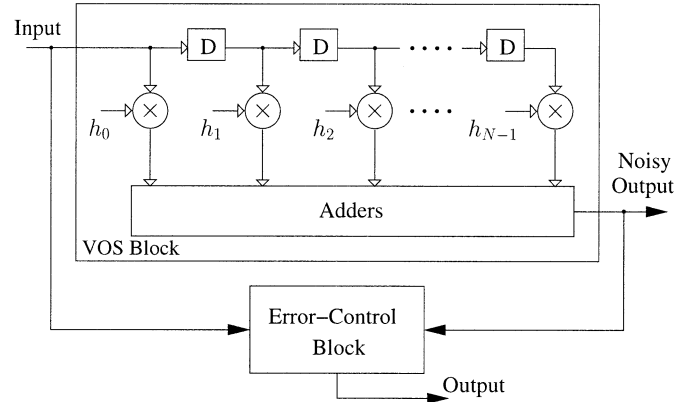
Fig. 1.   ANT-based low-power soft filtering scheme.

reduction techniques in the presence of noise. Fault-tolerant computing [19]–[23] improves reliability via introducing substantial hardware redundancy or employing sophisticated (and usually energy consuming) error-control schemes at the algorithmic/system level. In general, these techniques do not exploit domain-specific information for energy savings that is typically available in the design of signal processing and communication systems.

Our past work [24], [25] on determining lower bounds on energy-efficiency for DSM VLSI systems suggests that energy efficiency and reliability can be addressed jointly via *noise tolerance*. This motivates us to develop both circuit [26] and algorithmic noise-tolerance (ANT) techniques [27] as a practical method to achieve energy efficiency in the presence of noise while maintaining a specified level of performance. Furthermore, we have shown that ANT techniques have the potential of approaching the lower bounds on energy dissipation where aggressive design techniques create DSM noise-like behavior. Supply voltage scaling [28] is a commonly employed low-power technique that enables a linear reduction in static power dissipation and a quadratic reduction in dynamic power dissipation. Conventional voltage scaling schemes minimize power by reducing supply voltage V_{dd} to the point where critical path delays of the implementations just equal the throughput requirements. We refer to this supply voltage as $V_{dd-crit}$. Supply voltage overscaling (VOS) [27] reduces the voltage below $V_{dd-crit}$ in favor of additional energy reduction. Doing so, however, inevitably induces input-dependent *soft errors* due to delay violation. We have shown that ANT techniques employing low-complexity error-control schemes can effectively restore system performance while maintaining energy-efficiency. This overall approach of employing VOS in combination with ANT for low power is referred to as *soft digital signal processing (DSP)*, as illustrated in Fig. 1.

ANT techniques allow us to achieve energy reduction beyond that achievable with conventional techniques without

loss in system performance. It works best in the context of signal processing and communication systems, where system performance metrics are measured in terms of *signal-to-noise ratio* (SNR) and/or *bit-error rate* (BER). In order to guarantee substantial energy savings, an ANT technique should be effective in mitigating performance degradation while consuming minimal energy. Past work [27] reported a *prediction-based error-control* (PEC) scheme that is suitable for narrowband filters. For broadband signal processing, we proposed an *adaptive error-cancellation* (AEC) technique [29] via exploiting the correlation between the input signal and soft errors. In this paper, we build upon this AEC technique by proposing an AEC-based adaptive filtering scheme and a multi-input–multi-output (MIMO)-AEC scheme for low-power MIMO systems. MIMO signal processing is employed in many modern-day communication systems, such as crosstalk suppression in gigabit Ethernet 1000Base-T transceivers, multiuser detection and multi-antenna systems in wireless applications. Power dissipation is a critical concern for these systems due to intensive filtering computations being involved. The proposed MIMO-AEC exploits the inherent correlations in MIMO systems via MIMO decorrelating (MIMO-DECOR) to improve the energy-efficiency of AEC. We employ the proposed MIMO-AEC in the design of a low-power Gigabit Ethernet 1000Base-T device. Simulation results demonstrate 44.3%–25.2% reduction in energy overhead due to MIMO-DECOR and 69.1%–64.2% energy savings over conventional implementations at the same algorithmic performance.

The paper is organized as follows. In Section II, we review our past work on energy-optimum AEC. In Section III, we present the design strategies for AEC-based adaptive signal processing. In Section IV, we propose the MIMO-AEC technique for MIMO systems. Simulation results of Gigabit Ethernet 1000Base-T transceivers are provided in Section V.

II. ADAPTIVE ERROR-CANCELLATION (AEC)

In this section, we present preliminaries regarding VOS and ANT and review the past work on energy-optimum AEC (for broadband soft DSP implementations.

A. Algorithmic Noise-Tolerance

VOS exploits the relationship between supply voltage and circuit delay for power reduction. For the purpose of illustration, we assume that the critical path delay of a filter generating 22-bit outputs is equal to $22T_{a,V_{\mathrm{dd}}}$, where $T_{a,V_{\mathrm{dd}}}$ is the full adder delay at a voltage of V_{dd}. Thus, the minimal voltage $V_{\mathrm{dd-crit}}$ necessary for correct operation is determined by $T_s = 22T_{a,V_{\mathrm{dd-crit}}}$, where T_s is the sample period of the input. If the supply voltage is overscaled to $V_{\mathrm{dd-sub}} = V_{\mathrm{dd-crit}}/k_{\mathrm{vos}}$ [where $k_{\mathrm{vos}} > 1$ is the VOS factor (VOSF)] such that $T_{a,V_{\mathrm{dd-sub}}} = 1.2T_{a,V_{\mathrm{dd-crit}}}$, then $T_s \approx 18T_{a,V_{\mathrm{dd-sub}}}$. This indicates that, while the filter still functions correctly at the lower 18 least significant bits (LSBs) (assuming the use of LSB-first computation), the top four most significant bits (MSBs) of the output will be in error provided input patterns exciting the critical paths and other longer paths are applied.

Past work [27], [29] has shown that soft errors due to VOS can be corrected by low-complexity error-control techniques referred to as ANT. This leads to soft DSP implementations where

substantial energy reduction is made possible by VOS while the desired level of system performance is restored by ANT. An effective ANT technique is the one that is able to detect and correct errors that may arise in a comparatively large VOS block without incurring large overhead. The AEC technique [29] for broadband signal processing exploits the statistical relationship between the input and soft errors for error-control, as described below.

B. Energy-Optimum AEC

In the presence of soft error $e_s[n]$, the output $y_{\mathrm{vos}}[n]$ of an N-tap VOS filter $H(z)$ can be expressed as

$$y_{\mathrm{vos}}[n] = y[n] + e_s[n] = \sum_{j=0}^{N-1} h_j x[n-j] + e_s[n] \quad (1)$$

where h_j's are the coefficients of $H(z)$, $y[n]$ is the error-free output and $x[n]$ is the input.

AEC employs a low-complexity error-cancellation filter $H_c(z)$ that estimates the value of soft error $e_s[n]$ and then subtracts it from the output to mitigate the performance degradation. We observe that $e_s[n]$ is induced by the input samples $x[n], x[n-1], \ldots, x[n-N+1]$. Hence, it is possible to generate a statistical replica of soft errors from input samples by exploiting the correlation between the input signal and the soft-error signal. Given the fact that such correlation may be nonstationary due to variations in the process, temperature and input statistics, one effective way to do so is to use the *least mean square* (LMS) algorithm [30] that adaptively updates the coefficients $h_{c,j}$'s of the error canceller $H_c(z)$, as follows:

$$\widehat{e}_s[n] = \sum_{j=0}^{N-1} b_j h_{c,j}[n-1] x[n-j] \quad (2)$$

$$e_c[n] = e_s[n] - \widehat{e}_s[n] \quad (3)$$

$$h_{c,j}[n] = h_{c,j}[n-1] + \mu_c e_c[n]^* x[n-j] \quad (4)$$

where $\widehat{e}_s[n]$ is the estimate of $e_s[n]$, $e_c[n]$ denotes the estimation error, $e_c[n]^*$ is the complex conjugate of $e_c[n]$, μ_c is the step size, and b_j's $\in \{0,1\}$ are a control vector [32] of which the energy-optimum choice will be discussed later. It can be shown that by properly choosing the step size μ_c and b_j's, we are able to minimize the mean-squared estimation error, which is expressed as $\sigma_{e_c}^2 = E(e_c[n]^2)$. Thus, in the steady-state filtering operation, the output of an AEC-based filter can be expressed as

$$y_o[n] = y_{\mathrm{vos}}[n] - \widehat{e}_s[n] = y[n] + e_c[n]. \quad (5)$$

Comparing (5) and (1), we find that the performance degradation due to soft errors is mitigated. Fig. 2 illustrates the block diagram of the previously proposed AEC technique. The computations in (2) are done in the filter (**F**) block of the AEC and those in (4) are executed in the weight-update (**WUD**) block. The precisions of these two blocks are determined by the specifications on quantization errors, input statistics, convergence speed and algorithmic performance (such as the output SNR) [33]. Note that (2)–(4) define an auto-calibration phase where a predefined input signal is passed through the VOS filter $H(z)$ and a precomputed error-free output $y[n]$ is used as the desired signal. After the error canceller $H_c(z)$ has converged, the **WUD**-block can be powered-down and the multiplexer control signal can be
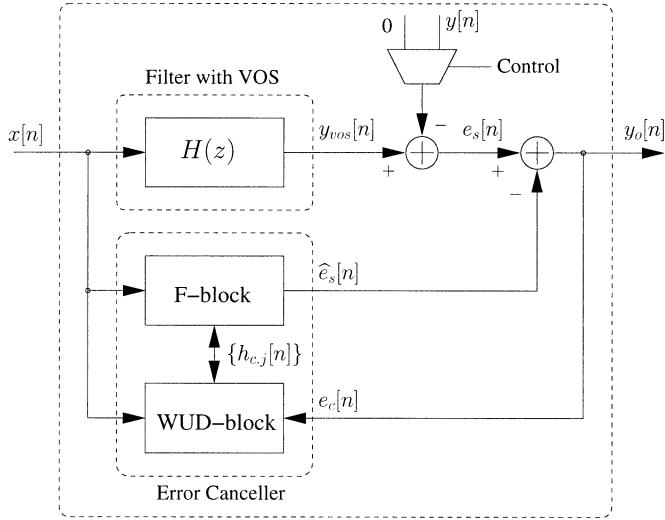
Fig. 2. Proposed ANT technique based on adaptive error-cancellation.

Fig. 3. AEC-based adaptive filter.

flipped so that $\widehat{e}_s[n]$ gets subtracted directly from the output $y_{\text{vos}}[n]$ thereby cancelling out the soft errors.

The vector $\underline{b} = \{b_0, b_1, \ldots, b_{N-1}\}$ in (2) determines the tradeoff between system performance and achievable energy savings. Specifically, $b_j = 0$ powers down the jth tap of $H_c(z)$ which alleviates the AEC overhead. Doing so, however, may degrade the effectiveness of error-cancellation. A systematic method has been proposed for deriving an energy-optimum solution $\underline{b}^*$ that minimizes the energy dissipation of the AEC-based filter while being subject to a prespecified level of algorithmic performance. Using the Lagrange multiplier method [31], the optimum solution $\underline{b}^*$ is obtained as [32]

$$b_j^* = \begin{cases} 1, & \text{if } \dfrac{\mathcal{E}_{F,j}}{h_{c,j}^2 \sigma_x^2} < \lambda^* \\[2mm] 0, & \text{if } \dfrac{\mathcal{E}_{F,j}}{h_{c,j}^2 \sigma_x^2} \geq \lambda^* \end{cases} \qquad (6)$$

where λ^* is the optimum *sensitivity vector* of the Lagrange multiplier, $\sigma_x{}^2$ the variance of the input signal $x[n]$ and $\mathcal{E}_{F,j}$ is the energy dissipation due to the jth tap of $H_c(z)$. Given the coefficient $h_{c,j}$, the value of $\mathcal{E}_{F,j}$ can be estimated via the weighted multiplier energy model [32]. The energy-optimum length N_c^{opt} of the resulting error canceller $H_c(z)$ can be expressed as

$$N_c^{\text{opt}} = \sum_{j=0}^{N-1} b_j^*. \qquad (7)$$

From (6), $b_j^* = 1$ if the jth tap of $H_c(z)$ has a large coefficient $h_{c,j}$ while consuming a relatively small energy $\mathcal{E}_{F,j}$. Otherwise, we can switch off the jth tap of $H_c(z)$. It was shown [29] that if the jth tap of the primary filter $H(z)$ has a coefficient with large magnitude, then the critical paths and other longer paths (which generate MSBs) get excited easily thereby creating a large soft-error component. This makes $h_{c,j}$ large which in turn implies $b_j^* = 1$. An important observation is that, as the bandwidth of $H(z)$ increases, the predominant contribution to the soft-error energy at the output will be from fewer taps of $H(z)$. This is because wideband filters have a narrow impulse response. Thus, more b_j^*'s will be zero resulting in a smaller
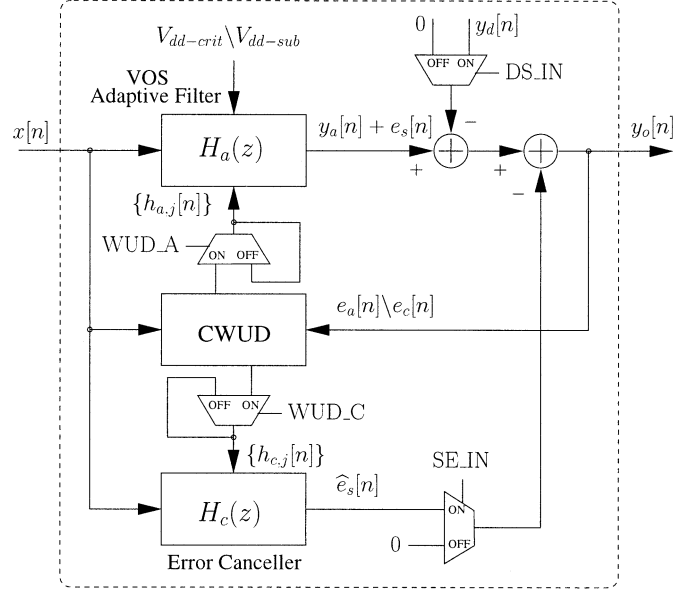
N_c^{opt}. This indicates that the proposed AEC technique is best suited for broadband signal processing.

In practice, we can avoid the computation of λ^* by powering down those taps in $H_c(z)$ starting with the tap with the largest value of $\mathcal{E}_{F,j}/(h_{c,j}^2 \sigma_x^2)$ and continuing until the prespecified algorithmic performance is violated. Past work [29] reported 43%–71% energy savings without performance loss in the context of single-input–single-output (SISO) systems.

III. AEC-BASED ADAPTIVE SIGNAL PROCESSING

In this section, we propose to apply the energy-optimum AEC in the design of low-power adaptive filters. We first develop an AEC-based adaptive filtering scheme in Section III-A and then present the performance analysis in Section III-B. The proposed AEC-based adaptive filtering scheme will be employed with MIMO-AEC for the design of low-power Gigabit Ethernet systems in Section V.

A. AEC-Based Adaptive Filter

The proposed AEC-based adaptive filtering scheme is shown in Fig. 3. Here both the primary adaptive filter, denoted by $H_a(z)$ and the error canceller $H_c(z)$ need to compute their coefficients adaptively. We assume that (a) the primary adaptive filter $H_a(z)$ and the error canceller $H_c(z)$ are calibrated separately and (b) the **WUD** block is powered-down during the steady-state filtering operation. Hence, a common weight-update (**CWUD**) block can be shared by both filters in order to reduce the hardware overhead of AEC. Note that the two-phase calibration of $H_a(z)$ and $H_c(z)$ is necessary as otherwise the estimation errors due to $H_a(z)$ and $H_c(z)$ become indistinguishable, thereby preventing the convergence of the two filters. In addition, for a given input signal, soft errors are dependent upon the coefficients of $H_a(z)$. Updating the coefficients of $H_a(z)$ changes the underlying soft-error model at every update cycle, thereby making it impossible for $H_c(z)$ to track. For these reasons, the calibration of $H_c(z)$ needs to be done after $H_a(z)$ has converged.

The operation of AEC-based LMS adaptive filters consists of three phases, as described below with reference to Fig. 3:

1) Filter Calibration Phase: During this phase, the supply voltage is set to $V_{\text{dd-crit}}$, control signals WUD_A and DS_IN are ON, WUD_C and SE_IN are OFF and a predefined training sequence is fed into $H_a(z)$. Note that during this phase soft error $e_s[n]$ is always zero. Hence, the coefficients $h_{a,j}$'s of $H_a(z)$ get updated by the error signal $e_a[n]$ between the filter output $y_a[n]$ and a precomputed desired signal $y_d[n]$, as follows:

$$y_a[n] = \sum_{j=0}^{N-1} h_{a,j}[n-1]x[n-j] \tag{8}$$

$$e_a[n] = y_a[n] - y_d[n] \tag{9}$$

$$h_{a,j}[n] = h_{a,j}[n-1] + \mu_a e_a[n]^* x[n-j]. \tag{10}$$

2) AEC Calibration Phase: During this phase, the supply voltage is overscaled to $V_{\text{dd-sub}}$ (whose value is determined by the algorithmic performance such as the output SNR [29]), control signals WUD_C, SE_IN and DS_IN are ON, while WUD_A is OFF. Due to VOS, soft errors start to appear at the output of $H_a(z)$. The coefficients h_{c,k_i}'s of the energy-optimum error canceller $H_c(z)$ are computed according to

$$\widehat{e}_s[n] = \sum_{i=0}^{N_c^{\text{opt}}-1} h_{c,k_i}[n-1]x[n-k_i] \tag{11}$$

$$e_c[n] = (e_s[n] + e_a[n]) - \widehat{e}_s[n] \tag{12}$$

$$h_{c,k_i}[n] = h_{c,k_i}[n-1] + \mu_c e_c[n]^* x[n-k_i] \tag{13}$$

where N_c^{opt} is given by (7) and $k_i = j$ if $b_j^* = 1$ in (6). Note that the error signal in (12) contains residual error $e_a[n]$ from the first phase [see (9)]. However, it will be shown later that $e_a[n]$ has a minor effect on the optimum configuration of $H_c(z)$ as described in (6) and (7).

3) Soft Filtering Phase: After $H_c(z)$ has converged, the supply voltage is kept at $V_{\text{dd-sub}}$, control signal SE_IN is ON while the others are OFF. The filter output $y_o[n]$ can be computed as

$$y_o[n] = y_a[n] + e_s[n] - \widehat{e}_s[n] \tag{14}$$

where $y_a[n]$ and $\widehat{e}_s[n]$ are given by (8) and (11), respectively, and $e_s[n]$ is the soft error due to VOS. This starts the steady-state filtering operation where significant energy reduction is achieved via VOS while the required algorithmic performance is guaranteed by AEC.

B. Performance Analysis

We now study the error-control performance of the proposed AEC-based adaptive filtering scheme. From (12), the error signal seen by $H_c(z)$ in the AEC calibration phase is composed of soft error $e_s[n]$ and the residual estimation error $e_a[n]$ from $H_a(z)$. However, it can be proved that the optimum Weiner–Hopf solutions for $H_c(z)$ and $H_a(z)$ are independent of each other.

To show this, we assume that the input $x[n]$ is a zero-mean and uncorrelated random signal and denote $y_d[n]$ as the desired signal for the adaptive filter $H_a(z)$. In the filter calibration phase, we obtain the optimum coefficients $h_{a,j}^{\text{opt}}$'s of $H_a(z)$ as [30]

$$h_{a,j}^{\text{opt}} = \frac{E\left(x[n-j]y_d[n]\right)}{\sigma_x^2} \tag{15}$$

where σ_x^2 is the variance of the input signal $x[n]$. Substituting $h_{a,j}^{\text{opt}}$ from (15) into (8) and (9), we obtain the residual estimation error $e_a^{\text{opt}}[n]$ as

$$e_a^{\text{opt}}[n] = \sum_{j=0}^{N-1} h_{a,j}^{\text{opt}} x[n-j] - y_d[n]. \tag{16}$$

In the AEC calibration phase, due to the presence of nonzero $e_a^{\text{opt}}[n]$, the optimum coefficients $h_{c,j}^{\text{opt}}$'s of the error canceller $H_c(z)$ can be expressed as

$$h_{c,j}^{\text{opt}} = \frac{E\left(\left(e_s[n] + e_a^{\text{opt}}[n]\right)x[n-j]\right)}{\sigma_x^2}$$
$$= \frac{E\left(e_s[n]x[n-j]\right)}{\sigma_x^2} + \frac{E\left(e_a^{\text{opt}}[n]x[n-j]\right)}{\sigma_x^2} \tag{17}$$

where $e_s[n]$ denotes the soft output error from the converged VOS filter $H_a(z)$. Note that the residual estimation error $e_a^{\text{opt}}[n]$ in the Weiner–Hopf solution is statistically orthogonal to the input signal $x[n]$ [30], i.e.,

$$\frac{E\left(e_a^{\text{opt}}[n]x[n-j]\right)}{\sigma_x^2} = 0. \tag{18}$$

Hence, $h_{c,j}^{\text{opt}}$'s in (17) are an unbiased optimum solution even if a nonzero $e_a^{\text{opt}}[n]$ is present.

The LMS calibrations given by (8)–(10) and (11)–(13) result in filter coefficients that approach their Weiner–Hopf solutions. It can be easily shown that after $H_a(z)$ has converged, the residual estimation error $e_a[n]$ can be expressed as

$$e_a[n] = e_a^{\text{opt}}[n] + \tilde{e}_a[n] \tag{19}$$

where $e_a^{\text{opt}}[n]$ is given by (16) and $\tilde{e}_a[n]$ denotes the input-dependent excess error which is statistically small.

From (12) and (19), the error canceller $H_c(z)$ is in fact cancelling $e_s[n] + \tilde{e}_a[n]$, as $e_a^{\text{opt}}[n]$ is orthogonal to the input signal $x[n]$ and therefore cannot be cancelled by $H_c(z)$. However, as $\tilde{e}_a[n]$ is much smaller than $e_s[n]$, it has a minor effect on the configuration of $H_c(z)$.

In practical systems, variations over time in temperature and physical channel parameters may occur which in turn will require us to recalibrate $H_a(z)$ and hence $H_c(z)$. The frequency of these recalibrations will depend upon the rate at which temperature and channel parameters change. For Gigabit Ethernet 1000Base-T systems of interest in this paper, the channel parameters and temperature are more or less constant. This is because these systems are located indoors with well-controlled ambient temperature. Hence, recalibration will be required on startup or once in several days if at all. In any case, the AEC-based adaptive filter can be recalibrated according to the procedure given in Section III-A.
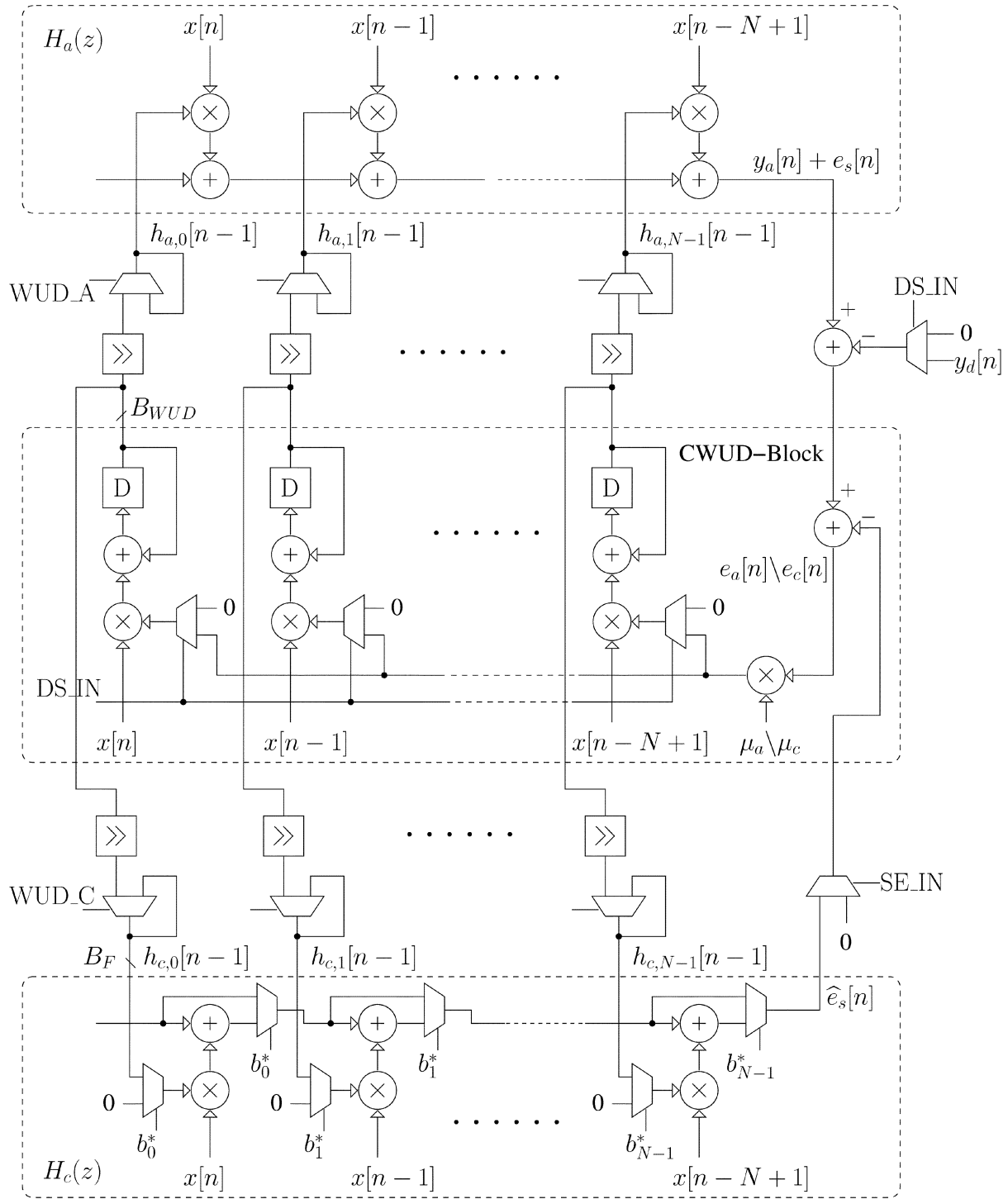
Fig. 4. VLSI architecture of the energy-optimum AEC-based adaptive filter.

Fig. 4 shows the architecture of an AEC-based adaptive filter. Simulation results in Section V demonstrate that the tap-length $N_c^{\mathbf{opt}}$ of the energy-optimum AEC is around $N/4$. Thus, the energy overhead incurred in AEC can be compensated easily by the energy savings obtained from VOS. Also, the AEC block has a shorter critical path, thus being error free even if the supply voltage of the AEC is made identical to that of the $H_a(z)$ for simplicity of implementation.

IV. MIMO-AEC FOR LOW-POWER MIMO SIGNAL PROCESSING

In this section, we extend the energy-optimum AEC to MIMO systems. In particular, we develop an MIMO-AEC technique that exploits the inherent correlations in MIMO systems via MIMO-DECOR transform to improve the energy-efficiency of AEC. As will be shown in Section V, the proposed MIMO-AEC

technique can achieve substantial energy savings in practical MIMO systems such as Gigabit Ethernet 1000Base-T transceivers. A matrix representation of MIMO systems is given in Section IV-A and the MIMO-AEC is proposed in Section IV-B. In Section IV-C, we derive the MIMO-DECOR transform for practical MIMO systems.

A. MIMO Model

Consider a generic p-input, q-output MIMO system composed of $p \times q$ adaptive or fixed-coefficient filters and expressed in matrix form as

$$
\begin{bmatrix} y_1[n] \\ y_2[n] \\ \cdots \\ y_q[n] \end{bmatrix} = \begin{bmatrix} \underline{\mathbf{h}}_{11} & \underline{\mathbf{h}}_{12} & \cdots & \underline{\mathbf{h}}_{1p} \\ \underline{\mathbf{h}}_{21} & \underline{\mathbf{h}}_{22} & \cdots & \underline{\mathbf{h}}_{2p} \\ \cdots & \cdots & \cdots & \cdots \\ \underline{\mathbf{h}}_{q1} & \underline{\mathbf{h}}_{q2} & \cdots & \underline{\mathbf{h}}_{qp} \end{bmatrix} \otimes_c \begin{bmatrix} \underline{\mathbf{x}}_1[n] \\ \underline{\mathbf{x}}_2[n] \\ \cdots \\ \underline{\mathbf{x}}_p[n] \end{bmatrix} \quad (20)
$$

where $\underline{\mathbf{x}}_j[n] = [x_j[n], x_j[n-1], \ldots, x_j[n-N+1]]^T$ is the jth input sequence, $\underline{\mathbf{h}}_{ij} = [h_{ij}[0], h_{ij}[1], \ldots, h_{ij}[N-1]]$ is the coefficient vector of the filter taking the jth input and generating the ith output, $y_i[n] = \sum_{j=1}^{p} \underline{\mathbf{h}}_{ij} \otimes_c \underline{\mathbf{x}}_j[n]$ is the ith output, and "$\otimes_c$" denotes the element-by-element convolution operation, i.e., $\underline{\mathbf{h}}_{ij} \otimes_c \underline{\mathbf{x}}_j[n] = \sum_{k=0}^{N-1} h_{ij}[k] x_j[n-k]$. A special case of (20) is a system with a diagonal transfer matrix (i.e., $\underline{\mathbf{h}}_{ij} = \underline{\mathbf{0}}$ for $i \neq j$) representing q independent SISO filtering operations, such as the channel equalizer in Gigabit Ethernet 1000Base-T transceivers (see Section V).

Henceforth, we refer to the filter with coefficient vector $\underline{\mathbf{h}}_{ij}$ as filter $\underline{\mathbf{h}}_{ij}$. Note that in practical MIMO systems the filters in (20) usually exhibit certain correlations in frequency or time domain. For example, the interference suppression scheme in a 1000Base-T device (see Section V) contains 12 near-end crosstalk (NEXT) cancellers, among which every three cancellers share the same input. These three cancellers have similar impulse responses, as they are designed to cancel three similar NEXT interferences which are induced by the same input signal on three spatially correlated crosstalk paths. Exploiting these inherent correlations allows us to develop effective energy reduction techniques as discussed below.

B. MIMO-AEC

We now present the low-power MIMO-AEC technique for MIMO signal processing systems. Assume that all the filters $\underline{\mathbf{h}}_{ij}$'s in (20) operate in parallel and have matched critical path delays. Energy reduction via VOS induces soft errors at all the filter outputs $y_i[n]$'s. This necessitates a bank of error cancellers, for which the Weiner–Hopf solution [30] is given by

$$
\begin{bmatrix} \underline{\mathbf{h}}_{c,11} & \underline{\mathbf{h}}_{c,12} & \cdots & \underline{\mathbf{h}}_{c,1p} \\ \underline{\mathbf{h}}_{c,21} & \underline{\mathbf{h}}_{c,22} & \cdots & \underline{\mathbf{h}}_{c,2p} \\ \cdots & \cdots & \cdots & \cdots \\ \underline{\mathbf{h}}_{c,q1} & \underline{\mathbf{h}}_{c,q2} & \cdots & \underline{\mathbf{h}}_{c,qp} \end{bmatrix} = E \left(\begin{bmatrix} e_{s1}[n] \\ e_{s2}[n] \\ \cdots \\ e_{sq}[n] \end{bmatrix} \begin{bmatrix} \underline{\mathbf{x}}_1[n] \\ \underline{\mathbf{x}}_2[n] \\ \cdots \\ \underline{\mathbf{x}}_p[n] \end{bmatrix}^T \right)
$$
$$
\cdot E \left(\begin{bmatrix} \underline{\mathbf{x}}_1[n] \\ \underline{\mathbf{x}}_2[n] \\ \cdots \\ \underline{\mathbf{x}}_p[n] \end{bmatrix} \begin{bmatrix} \underline{\mathbf{x}}_1[n] \\ \underline{\mathbf{x}}_2[n] \\ \cdots \\ \underline{\mathbf{x}}_p[n] \end{bmatrix}^T \right)^{-1} \quad (21)
$$

where $\underline{\mathbf{h}}_{c,ij}$ is the coefficient vector of the error canceller for the filter $\underline{\mathbf{h}}_{ij}$, and $e_{si}[n]$ is the soft error at the ith output $y_i[n]$. From (20), $e_{si}[n]$ contains p soft-error components, i.e.,

$$
e_{si}[n] = \sum_{j=1}^{p} e_{si,j}[n] \quad (22)
$$

where $e_{si,j}[n]$ denotes the soft error induced by $\underline{\mathbf{x}}_j[n]$ in the VOS filtering operation $\underline{\mathbf{h}}_{ij} \otimes_c \underline{\mathbf{x}}_j[n]$.

Assume that the input sequences $\underline{\mathbf{x}}_j[n]$'s are zero-mean and from independent data sources, which is typical for practical MIMO systems. Thus, $e_{si,j}[n]$ in (22) is uncorrelated to $\underline{\mathbf{x}}_k[n]$ for $k \neq j$, i.e., $E(e_{si,j}[n] \underline{\mathbf{x}}_k[n]^T) = \underline{\mathbf{0}}$. Accordingly, the solution of $\underline{\mathbf{h}}_{c,ij}$ in (21) can be expressed as

$$
\underline{\mathbf{h}}_{c,ij} = \frac{E \left(e_{si,j}[n] \underline{\mathbf{x}}_j[n]^T \right)}{\sigma_{x_j}^2} \quad (23)
$$

where $\sigma_{x_j}^2$ is the variance of $\underline{\mathbf{x}}_j[n]$. Note that the result given by (23) is the same as that for a SISO filter. Hence, we can decouple the $p \times q$ error cancellers $\underline{\mathbf{h}}_{c,ij}$'s and implement each of them independently via the energy-optimum AEC given in Section III. We denote this approach as *direct-AEC*, as shown in Fig. 5(a).

While the energy-optimum AEC guarantees the minimum energy overhead for an individual error canceller, the direct-AEC scheme consisting of $p \times q$ independent error cancellers, one for each VOS filter in (20), may not be energy-efficient. This is due to the fact that the possible correlations among the original filters $\underline{\mathbf{h}}_{ij}$'s may introduce computational redundancies. In order to further improve energy-efficiency, we propose an algorithm transformation denoted as MIMO-DECOR. In contrast with the direct-AEC, the AEC scheme employing MIMO-DECOR for energy optimization is referred to as MIMO-AEC.

C. MIMO-DECOR

Decorrelating (DECOR) transform [35] was studied previously for narrowband SISO filters. It employs the fact that the difference between the adjacent coefficients of a filter is typically less in magnitude, thereby requiring less hardware complexity and power dissipation in the implementation. The motivation for the MIMO-DECOR proposed in this paper is that for filters in a MIMO system with correlated time-frequency characteristics (i.e., bandwidths, impulse responses, etc.), a smaller precision and fewer taps might be sufficient for representing the difference between these filters than those for themselves. Thus, we can employ the proposed MIMO-DECOR to shorten some critical paths so that some filters in the MIMO system will become error free during VOS. This helps to reduce the number of error cancellers, thereby reducing the overhead of noise-tolerance. Note that the proposed MIMO-DECOR differs from the previous work [35], [36] in that it is employed to reduce the correlations among the filters in a MIMO system. These filters can be either wide-band or narrow-band.

In its most general form, the MIMO-DECOR can be expressed as

$$
[\tilde{\underline{\mathbf{y}}}[n]]_{q \times 1} = \left[\mathcal{T} \left([\underline{\mathbf{h}}]_{q \times p} \right) \right]_{q \times p} \otimes_c [\underline{\mathbf{x}}[n]]_{p \times 1} \quad (24)
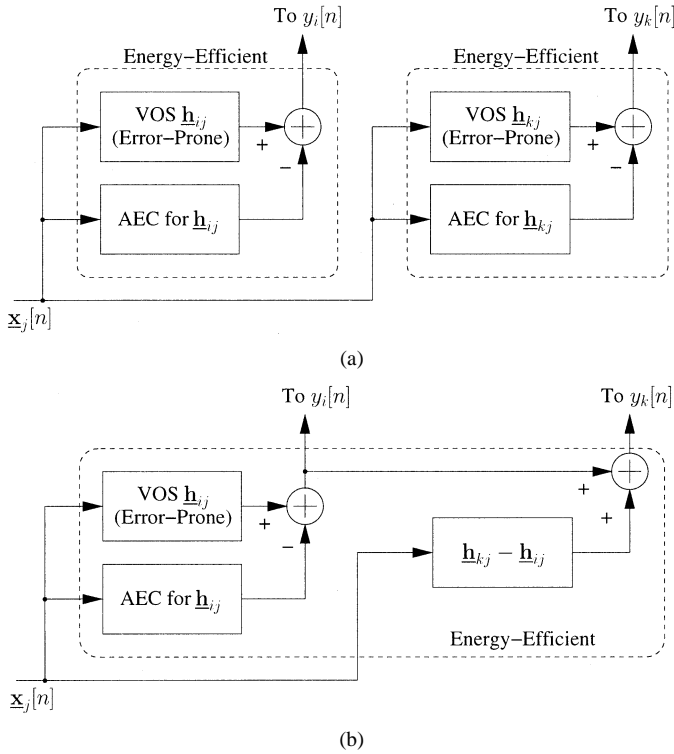$$

Fig. 5.   Proposed MIMO-AEC technique. (a) Direct-AEC. (b) MIMO-AEC with MIMO-DECOR.

$$\left[\mathbf{y}[n]\right]_{q\times1} = \left[\mathcal{T}^{-1}\left(\left[\tilde{\mathbf{y}}[n]\right]_{q\times1}\right)\right]_{q\times1} \tag{25}$$

where $\mathcal{T}(\cdot)$ denotes the MIMO-DECOR transform, $[\tilde{\mathbf{y}}[n]]_{q\times1}$ is the output vector of the transformed system, $[\underline{\mathbf{h}}]_{q\times p}$, $[\underline{\mathbf{x}}[n]]_{p\times1}$ and $[\mathbf{y}[n]]_{q\times1}$ are the short forms for the transfer matrix, inputs and outputs, respectively, of the original MIMO system (20). An inverse MIMO-DECOR transform, denoted by $\mathcal{T}^{-1}(\cdot)$, is employed to convert the output vector $[\tilde{\mathbf{y}}[n]]_{q\times1}$ back to the desired $[\underline{\mathbf{y}}[n]]_{q\times1}$.

To achieve the original goal of energy reduction, the MIMO-DECOR transform and its inverse should be simple so that the energy overhead incurred is small. In what follows, we will derive a MIMO-DECOR transform where $\mathcal{T}$ and $\mathcal{T}^{-1}$ are q-by-q matrices, resulting in matrix operations in (24) and (25). It will be shown that the effectiveness of MIMO-AEC is determined by the statistical properties of original MIMO systems. An energy-efficient MIMO-AEC scheme can be easily devised for practical MIMO systems having correlated time-frequency characteristics.

Consider a general class of MIMO systems where the filters with the same input [say, filters $\underline{\mathbf{h}}_{ij}$ and $\underline{\mathbf{h}}_{kj}$ in (20)] have correlated time-frequency characteristics (i.e., bandwidths, impulse responses, etc.). This is typical for practical MIMO systems, e.g., Gigabit Ethernet 1000Base-T transceivers. We note that the correlated impulse responses imply a smaller precision for representing the difference between the coefficients $\underline{\mathbf{h}}_{ij}$ and $\underline{\mathbf{h}}_{kj}$ than that for $\underline{\mathbf{h}}_{ij}$ and $\underline{\mathbf{h}}_{kj}$ themselves. In addition, fewer taps might be sufficient for representing $(\underline{\mathbf{h}}_{ij} - \underline{\mathbf{h}}_{kj})$. Therefore, we can compute the outputs of these two filters alternatively by using the following filtering scheme

$$y_{ij}[n] = \underline{\mathbf{h}}_{ij} \otimes_c \underline{\mathbf{x}}_j[n] \tag{26}$$

$$\Delta y[n] = \left(\underline{\mathbf{h}}_{kj} - \underline{\mathbf{h}}_{ij}\right) \otimes_c \underline{\mathbf{x}}_j[n] \tag{27}$$

$$y_{kj}[n] = y_{ij}[n] + \Delta y[n] \tag{28}$$

where $y_{ij}[n]$ and $y_{kj}[n]$ are the outputs of the filters $\underline{\mathbf{h}}_{ij}$ and $\underline{\mathbf{h}}_{kj}$, respectively. Obviously, the critical path delay of (27) is much less than that of (26) due to its reduced complexity. This also leads to additional energy savings that easily compensate for the overhead of extra computations in (28). Moreover, when applying VOS for further energy reduction, only (26) will induce soft output errors and thus require an error canceller, whereas (27) and (28) will be error free (if their critical paths are sufficiently short, which is true for NEXT cancellers in 1000Base-T transceivers). This reduces the AEC overhead to just one error canceller as compared to two in a direct-AEC implementation, as illustrated in Fig. 5.

The effectiveness of the above filtering scheme is determined by the relative configuration of $\underline{\mathbf{h}}_{ij}$ and $\underline{\mathbf{h}}_{kj}$. If $\underline{\mathbf{h}}_{ij}$ and $\underline{\mathbf{h}}_{kj}$ are identical under a maximum correlation scenario, then $(\underline{\mathbf{h}}_{kj} - \underline{\mathbf{h}}_{ij}) = \underline{\mathbf{0}}$, resulting in the maximum energy savings as the computations in (27)–(28) can be avoided. On the contrary, if $\underline{\mathbf{h}}_{ij}$ and $\underline{\mathbf{h}}_{kj}$ are so different (uncorrelated) that the complexity of (27) is comparable to that of (26), then no energy savings can be obtained over direct-AEC implementations. As will be shown in Section V, for practical MIMO systems such as 1000Base-T transceivers, the computations in (27) are typically simple enough to guarantee substantial energy savings via MIMO-AEC.

The filtering scheme given by (26)–(28) can be equally applied to other filters in (20) as well. Let $i = 1$, $k = 2, \ldots, q$ and $j = 1, \ldots, p$, we obtain the following MIMO-DECOR transform as:

$$\left[\mathcal{T}\left([\underline{\mathbf{h}}]_{q\times p}\right)\right]_{q\times p}$$
$$= \begin{bmatrix} 1 & 0 & \cdots & 0 \\ -1 & 1 & \cdots & 0 \\ \cdots & \cdots & \cdots & \cdots \\ -1 & 0 & \cdots & 1 \end{bmatrix}_{q\times q} \cdot [\underline{\mathbf{h}}]_{q\times p}$$
$$= \begin{bmatrix} \underline{\mathbf{h}}_{11} & \underline{\mathbf{h}}_{12} & \cdots & \underline{\mathbf{h}}_{1p} \\ (\underline{\mathbf{h}}_{21} - \underline{\mathbf{h}}_{11}) & (\underline{\mathbf{h}}_{22} - \underline{\mathbf{h}}_{12}) & \cdots & (\underline{\mathbf{h}}_{2p} - \underline{\mathbf{h}}_{1p}) \\ \cdots & \cdots & \cdots & \cdots \\ (\underline{\mathbf{h}}_{q1} - \underline{\mathbf{h}}_{11}) & (\underline{\mathbf{h}}_{q2} - \underline{\mathbf{h}}_{12}) & \cdots & (\underline{\mathbf{h}}_{qp} - \underline{\mathbf{h}}_{1p}) \end{bmatrix} \tag{29}$$

and the corresponding inverse MIMO-DECOR transform is given by

$$\left[\mathcal{T}^{-1}\left([\tilde{\mathbf{y}}[n]]_{q\times1}\right)\right]_{q\times1}$$
$$= \begin{bmatrix} 1 & 0 & \cdots & 0 \\ 1 & 1 & \cdots & 0 \\ \cdots & \cdots & \cdots & \cdots \\ 1 & 0 & \cdots & 1 \end{bmatrix}_{q\times q} \cdot [\tilde{\mathbf{y}}[n]]_{q\times1}$$
$$= \begin{bmatrix} \tilde{y}_1[n] \\ (\tilde{y}_2[n] + \tilde{y}_1[n]) \\ \cdots \\ (\tilde{y}_q[n] + \tilde{y}_1[n]) \end{bmatrix} \tag{30}$$
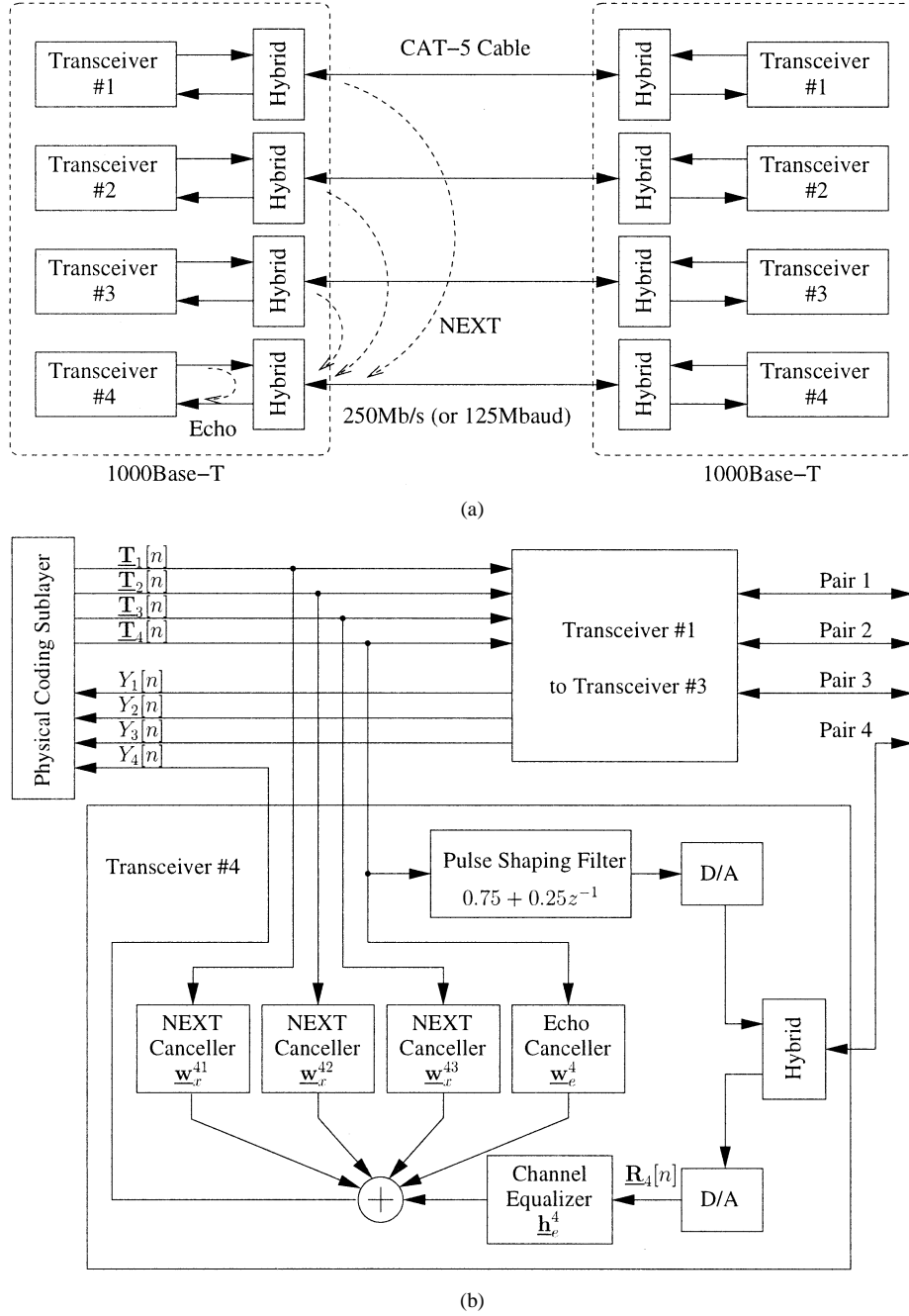
Fig. 6. 1000Base-T transmission scheme. (a) Signal impairments in one transceiver. (b) Block diagram of signal recovery scheme.

where $[\tilde{\underline{\mathbf{y}}}[n]]_{q \times 1}$ is given by (24). Obviously, $\mathcal{T} \cdot \mathcal{T}^{-1} = \mathbf{I}_{q \times q}$, where $\mathbf{I}_{q \times q}$ is an identity matrix. Hence, the outputs of inverse MIMO-DECOR transform equal the desired outputs.

From (29) and (30), the MIMO-DECOR transform involves coefficient precomputation and the inverse MIMO-DECOR transform adds up the differential outputs of the transformed system to give the desired ones. It is easy to see that both transforms incur very small overhead and are easy to implement. In addition, there are $(q-1) \times p$ out of $q \times p$ filters in the transformed system (29) performing low-complexity filtering. As a result, the number of error cancellers needed can be reduced from $q \times p$ for direct-AEC to only p for MIMO-AEC. In summary, the proposed MIMO-AEC technique achieves substantial energy reduction via (a) MIMO-DECOR resulting

in low-complexity filtering, (b) VOS, and (c) energy-optimum AEC for restoring algorithmic performance. Section V presents the results of energy savings obtained via the MIMO-AEC technique.

V. APPLICATION TO GIGABIT ETHERNET

In this section, we study the performance of the proposed MIMO-AEC technique in a Gigabit Ethernet communication system. Power reduction is important for such high-speed and high-complexity application due to reducing the cost of packaging and cooling and improving reliability. We first give an overview of Gigabit Ethernet 1000Base-T standard and then employ the MIMO-AEC technique to design a low-power 1000Base-T device.

A. 1000Base-T Transceivers

Gigabit Ethernet is a new generation of high-bandwidth data interface over copper medium for local area networks (LAN). The 1000Base-T standard defines connections between switches/repeaters and data terminal equipments (DTE) such as desktop terminals. As illustrated in Fig. 6, the 1000Base-T transmission scheme specifies a 1000Mb/s, full duplex data throughput achieved by using four pairs of wire in Category 5 (CAT-5) cable, each pair transmitting a 250Mb/s data stream encoded into a four-dimension (4-D) five-level $\{-2, -1, 0, 1, 2\}$ pulse amplitude modulation (4-D PAM-5) signal constellation. The interested reader is referred to [1] for a detailed discussion of 4-D PAM-5 modulation scheme.

Each 1000Base-T device contains four identical transceivers, one for each pair of physical wire. The bidirectional data transmission on the same wire is made possible by hybrid circuits. On the transmit side, the outgoing data stream is processed by a pulse shaping filter $0.75 + 0.25z^{-1}$ to limit the high-frequency radiation of the transmitted signal within FCC requirements. On the receive side, each receiver confronts a physical channel of minimum 100m CAT-5 cable. As shown in Fig. 6(a), the three major causes of signal distortion encountered are propagation loss (due to channel attenuation), echo noise (generated by a self-returned signal due to impedance mismatch in hybrid circuits) and NEXT noise (caused by near-end crosstalk between adjacent wires). The detailed description of physical mechanisms of these impairments can be found in [37]. The IEEE Standard 802.3ab [1] specifies the models for the worst-case noise environment as

$$L_P(f) = 2.1 f^{0.529} + \frac{0.4}{f} \tag{31}$$

$$L_N(f) = 27.1 - 16.8 \log_{10}\left(\frac{f}{100}\right) \tag{32}$$

$$L_E(f) = \begin{cases} 15, & 1 \leq f < 20 \\ 15 - 10 \log_{10}\left(\frac{f}{20}\right), & 20 \leq f \leq 100 \end{cases} \tag{33}$$

where $1 \leq f \leq 100$ is the frequency expressed in MHz, $L_P(f)$, $L_N(f)$ and $L_E(f)$, all expressed in dB/100 m, are the squared magnitude of the propagation loss, NEXT, and echo transfer function, respectively.

The 1000Base-T data transmission requires a BER $\leq 10^{-10}$. Using 4-D PAM-5 modulation scheme, the SNR at the slicer for achieving this BER is 19.3 dB. To overcome considerable signal distortion caused by echo, NEXT, cable attenuation and dispersion, advanced digital signal processing and filtering techniques are needed for signal recovery. Fig. 6(b) depicts the block diagram of a 1000Base-T device which consists of four identical transceivers operating simultaneously at 125 Mbaud. At each receiver, the digital output of the A/D converter is first filtered by a feed-forward equalizer (FFE) to remove the intersymbol interference (ISI) introduced by the channel. As each received signal is also corrupted by one echo and three NEXT interferences from the adjacent wires, one echo canceller and three NEXT cancellers are needed correspondingly to perform interference suppression. In total, each 1000Base-T device requires four FFEs, four echo cancellers and twelve NEXT cancellers, all of which are LMS adaptive filters. This involves intensive

TABLE I
DESIGN SPECIFICATIONS FOR THE ENERGY-OPTIMUM AEC-BASED FILTERS

	FFE	AEC for FFE	Echo Canceller	AEC for Echo	NEXT Canceller	AEC for NEXT
Tap #	16	5	64	15	70	18
B_{INPUT}	$8b$	$8b$	$3b$	$3b$	$3b$	$3b$
B_F	$10b$	$5b$	$12b$	$8b$	$10b$	$8b$
B_{WUD}	$12b$	$12b$	$14b$	$14b$	$14b$	$14b$
T_{cp}	$26T_a$	$19T_a$	$25T_a$	$17T_a$	$25T_a$	$19T_a$

TABLE II
DESIGN SPECIFICATIONS AND ENERGY SAVINGS FOR THE DIFFERENTIAL NEXT CANCELLERS USING MIMO-DECOR

$L_N^{\min}$	$5dB$	$10dB$	$15dB$	$20dB$
Tap #	52	56	59	63
bit-width	$5b$	$5b$	$6b$	$7b$
T_{cp}	$18T_a$	$18T_a$	$19T_a$	$20T_a$
Reduction in AEC Energy Overhead	44.3%	42.6%	37.1%	25.3%

filtering operations which necessitate effective energy reduction techniques to alleviate power dissipation.

B. Simulation Results

We describe the signal recovery scheme on the receive side of a 1000Base-T device [see Fig. 6(b)] as a MIMO system, which is expressed as

$$\begin{bmatrix} Y_1[n] \\ Y_2[n] \\ Y_3[n] \\ Y_4[n] \end{bmatrix} = \begin{bmatrix} \mathbf{h}_e^1 & 0 & 0 & 0 \\ 0 & \mathbf{h}_e^2 & 0 & 0 \\ 0 & 0 & \mathbf{h}_e^3 & 0 \\ 0 & 0 & 0 & \mathbf{h}_e^4 \end{bmatrix} \otimes_c \begin{bmatrix} \mathbf{R}_1[n] \\ \mathbf{R}_2[n] \\ \mathbf{R}_3[n] \\ \mathbf{R}_4[n] \end{bmatrix}$$
$$- \begin{bmatrix} \mathbf{w}_e^1 & \mathbf{w}_x^{12} & \mathbf{w}_x^{13} & \mathbf{w}_x^{14} \\ \mathbf{w}_x^{21} & \mathbf{w}_e^2 & \mathbf{w}_x^{23} & \mathbf{w}_x^{24} \\ \mathbf{w}_x^{31} & \mathbf{w}_x^{32} & \mathbf{w}_e^3 & \mathbf{w}_x^{34} \\ \mathbf{w}_x^{41} & \mathbf{w}_x^{42} & \mathbf{w}_x^{43} & \mathbf{w}_e^4 \end{bmatrix} \otimes_c \begin{bmatrix} \mathbf{T}_1[n] \\ \mathbf{T}_2[n] \\ \mathbf{T}_3[n] \\ \mathbf{T}_4[n] \end{bmatrix} \tag{34}$$

where $\{Y_1[n], Y_2[n], Y_3[n], Y_4[n]\}$ is the recovered 4-D PAM-5 signal, $\mathbf{T}_i[n]$ and $\mathbf{R}_i[n]$ are the transmitted and received signals, respectively, at the ith transceiver, $\mathbf{h}_e^i$, $\mathbf{w}_e^i$, and $\mathbf{w}_x^{ij}$ denote the FFE, echo canceller and NEXT canceller (to cancel the NEXT interference generated by the jth transmitter), respectively, for the ith receiver. Note that the first term on the right side of (34) represents channel equalization which involves independent SISO filtering, whereas the second term describes the MIMO interference suppression scheme. In what follows, we employ the proposed AEC to reduce the power dissipation of signal recovery scheme (34). In particular, we apply the MIMO-AEC for the MIMO interference suppression scheme.

We assume that the SNR requirements for the FFE, echo cancellation and NEXT cancellation are 25 dB, 28 dB, and 30 dB, respectively. This results in a 21 dB SNR at $Y_i[n]$, which is 1.7 dB higher than the minimum of 19.3 dB necessary for achieving a BER of 10^{-10}. From (34), the FFE and echo cancellation involve independent SISO filtering operations,
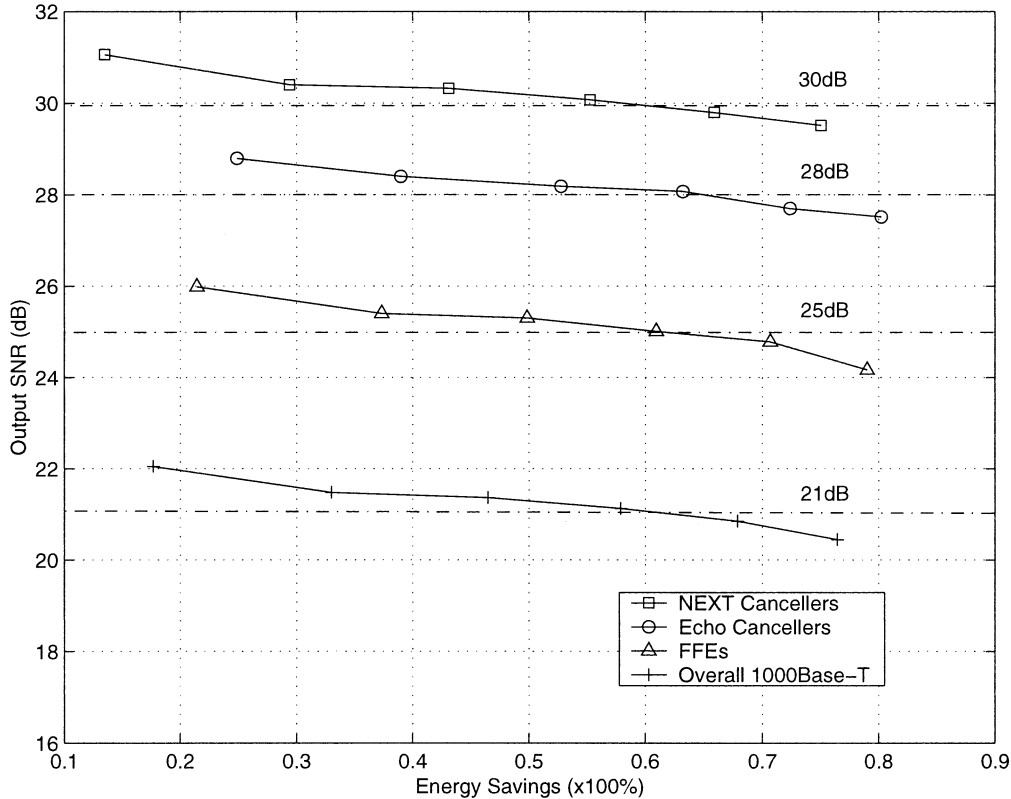
Fig. 7. Energy savings via direct-AEC.

thus enabling direct-AEC for energy reduction. Note that these filters are LMS adaptive filters which can be implemented using the AEC-based adaptive filtering scheme proposed in Section III. As mentioned before, every three NEXT cancellers with the same input (e.g., $\underline{\mathbf{w}}_x^{14}$, $\underline{\mathbf{w}}_x^{24}$, and $\underline{\mathbf{w}}_x^{34}$ with $\underline{\mathbf{R}}_4[n]$ as their input) have correlated impulse responses, thereby enabling MIMO-AEC to further improve the energy-efficiency. In practical 1000Base-T systems, the frequency responses of NEXT interferences vary away from the bound given by (32) due to physical variations of CAT-5 cable. An estimate of these variations can be obtained from experiments in the field. In this paper, we emulate these variations by introducing a disturbance $\Delta L_N(f)$ uniformly distributed between $[-L_N^{\min}, 0]$ onto the transfer function $L_N(f)$. Thus, an instance of NEXT interference with a frequency response of $L_N(f) + \Delta L_N(f)$ is generated and utilized to calibrate the associated NEXT canceller.

We use a full adder with $T_a = 0.3$ ns at $V_{\mathrm{dd-crit}} = 2.5$ V to implement these filters in a 0.25-μm CMOS technology. All the simulations employ the filter architecture shown in Fig. 1, where two's complement carry–save Baugh–Wooley multipliers [38] and ripple–carry tree-style adders are being employed. It was found (see Table I) that the critical path delays T_{cp}'s for the FFEs, echo cancellers and NEXT cancellers are no more than $26T_a$. Thus, these filters meet the sample period requirement which is 8 ns for 1000Base-T devices. We employ a logic level simulation [29] to detect delay violations due to VOS on every path to the filter output given a sequence of inputs. Thus, all paths and not just the critical paths are included. If the propagation delay on a path is larger than the sample period requirement, the corresponding output will not

be able to settle to its new value and instead retain its previous value thereby resulting in an output error. The output SNR is calculated by averaging over the entire input data set. In our simulations, we assume stationary variations in temperature, process and channel parameters. Thus, the energy dissipation is dominated by steady-state energy dissipation referred to the energy consumed after the adaptive filters have converged. On average, we observe a convergence time of 4000 samples for the primary filter $H_a(z)$ and 650 samples for the error canceller $H_c(z)$. The energy dissipation is obtained via the gate-level simulation tool MED [39] for a 0.25-μm CMOS technology. MED uses a gate-level model that includes load capacitances from a physical layout of the cell and its fan-out but not the interconnect. Note that absolute accuracy of MED is not important here as we are interested in relative comparisons between conventional and proposed systems.

Fig. 7 plots the energy-performance tradeoffs achieved via direct-AEC for an individual FFE, echo canceller, NEXT canceller, as well as for the 1000Base-T device consisting of four FFEs, four echo cancellers and twelve NEXT cancellers. It is shown that in comparison with conventional implementations, energy savings of 63.1%, 65.7%, and 59.5% are achieved for the FFEs, echo cancellers and NEXT cancellers, respectively, at the desired SNR. The overall energy savings for the 1000Base-T device is found around 60.2% at 21 dB SNR. These energy savings are obtained at $k_{\mathrm{vos}} \approx 1.7$ and $T_{a,V_{\mathrm{dd-sub}}} \approx 0.4$ ns. Table I provides design specifications for these filters and the associated AECs. As indicated, the energy-optimum AECs have a critical path delay of less than $20T_a$, thus being error-free ($T_{\mathrm{cp}} < 8$ ns) at $V_{\mathrm{dd-sub}}$. These results are consistent with those obtained for frequency-selective filters in [29].
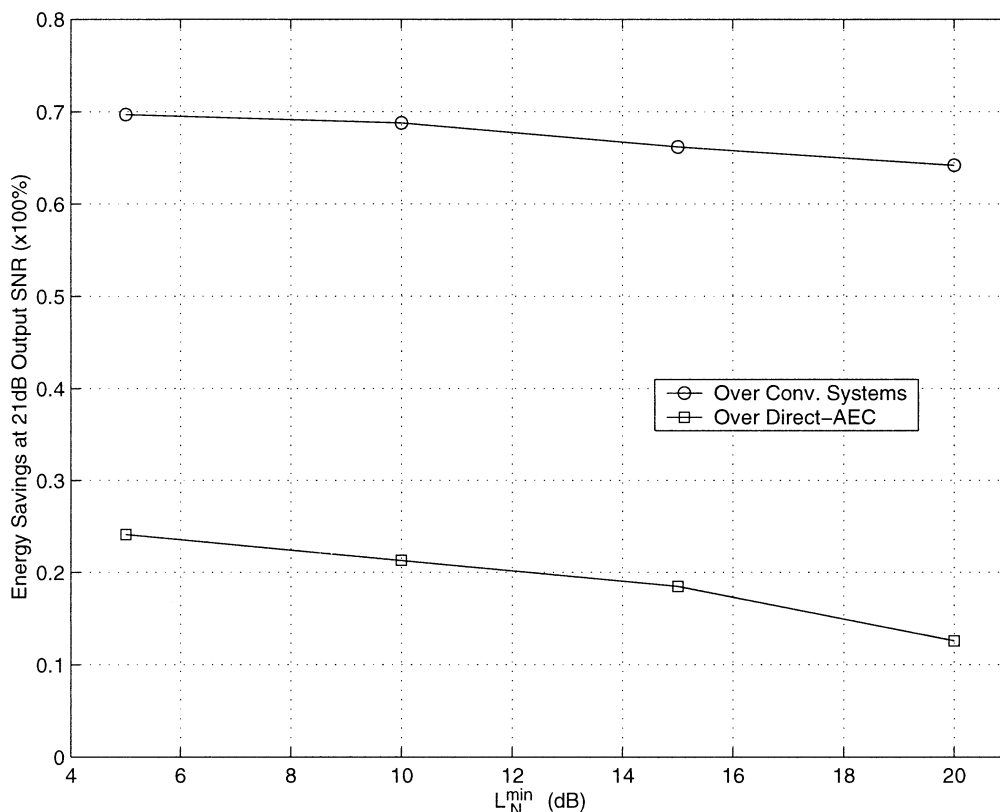
Fig. 8.   Energy savings via MIMO-AEC.

Further energy reduction can be obtained for NEXT cancellation via the proposed MIMO-AEC, resulting in four conventional NEXT cancellers and eight low-complexity differential NEXT cancellers due to MIMO-DECOR [see (26)–(28)]. In addition, the number of AECs needed is reduced from twelve to only four. As indicated in Table II, a strong correlation (e.g., $L_N^{\min} = 5$ dB) among the NEXT cancellers enables a large reduction in the AEC energy overhead (44.3%), otherwise the reduction in AEC energy overhead is small and the differential NEXT cancellers may become error prone at VOS. This is consistent with our discussion in Section IV. For practical 1000Base-T transceivers where $L_N^{\min}$ is typically around 10–15 dB, the MIMO-AEC leads to about 40% reduction in AEC energy overhead. Also shown in Fig. 8, a 1000Base-T device employing the MIMO-AEC can achieve energy savings of 22.1%–12.6% over direct-AEC implementations and 69.1%–64.2% over conventional implementations at the same output SNR.

VI. DISCUSSIONS AND CONCLUSIONS

In this paper, we have presented a new ANT technique, denoted as MIMO-AEC, for the design of low-power MIMO signal processing systems. VOS is an integral part of the proposed low-power strategy. Thus, voltage regulation circuits [34], which are an integral part of all microprocessors using dynamic voltage scaling (DVS), are required. Our approach requires a change in the voltage only during calibration phase. For applications such as Gigabit Ethernet 1000Base-T where the variations in temperature and channel parameters are very slow, the calibration phase requires negligible time compared to the soft filtering phase. Hence, the power in the voltage regulation circuitry is assumed to be negligible.

One can ask the question whether VOS is feasible as the nominal supply voltages scale with future technologies. The answer is in the affirmative because process designers set the nominal supply voltage to be about three times the device threshold voltage. This is done in order to have devices with sufficient current drive from one technology generation to the next. This condition, however, is not a requirement for the application of ANT. Given this constraint, it is always possible to voltage overscale as there is sufficient room between the device threshold voltage and the nominal supply voltage.

While we have considered ANT for finite impulse response (FIR) filtering in this paper, many other ANT techniques remain to be discovered for a host of DSP algorithms such as the FFT, DCT, IIR filters, etc.. One problem that remains to be solved is to quantify the relationship between VOS and soft-error statistics. This relationship is a function of the arithmetic unit architecture and to some extent the process technology itself.

REFERENCES

[1] *IEEE Standard 802.3ab 1000Base-T UTP Gigabit Ethernet*, 1999.
[2] R. He, N. Nazari, and S. Sutardja, "A DSP based receiver for 1000Base-T PHY," in *Proc. 2001 Int. Solid-State Circuits Conf. (ISSCC)*, San Francisco, CA, Feb. 2001, pp. 308–309.
[3] J. M. Cioffi, V. Oksman, J. -J. Werner, T. Pollet, P. M. P. Spruyt, J. S. Chow, and K. S. Jacobsen, "Very-high-speed digital subscriber lines," *IEEE Commun. Mag.*, vol. 37, pp. 72–79, Apr. 1999.
[4] M. Gagnaire, "An overview of broad-band access technologies," *Proc. IEEE*, vol. 85, pp. 1958–1972, Dec. 1997.
[5] R. Pandya, D. Grillo, E. Lycksell, P. Mieybegue, H. Okinaka, and M. Yabusaki, "IMT-2000 standards: Network aspects," *IEEE Pers. Commun.*, pp. 10–29, Aug. 1997.

[6] R. D. Carsello, R. Meidan, S. Allpress, F. O'Brien, J. A. Tarallo, N. Ziesse, A. Arunachalam, J. M. Costa, E. Berruto, R. C. Kirby, A. Maclatchy, F. Watanabe, and H. Xia, "IMT-2000 standards: Radio aspects," *IEEE Pers. Commun.*, pp. 30–40, Aug. 1997.

[7] A. P. Chandrakasan and R. W. Brodersen, "Minimizing power consumption in digital CMOS circuits," *Proc. IEEE*, vol. 83, pp. 498–523, Apr. 1995.

[8] J. D. Meindl, "Low power microelectronics: Retrospect and prospect," *Proc. IEEE*, vol. 83, pp. 619–635, Apr. 1995.

[9] D. A. Parker and K. K. Parhi, "Low-area/power parallel FIR digital filter implementations," *J. VLSI Signal Processing*, vol. 17, pp. 75–92, Sept. 1997.

[10] B. Davari, R. H. Dennard, and G. G. Shahidi, "CMOS scaling for high-performance and low power—The next ten years," *Proc. IEEE*, vol. 83, pp. 595–606, Apr. 1995.

[11] K. L. Shepard and V. Narayanan, "Noise in deep submicron digital design," in *Proc. '96 IEEE/ACM Int. Conf. Computer-Aided Design, (ICCAD)*, San Jose, CA, Nov. 1996, pp. 524–531.

[12] P. Larsson and C. Svensson, "Noise in digital dynamic CMOS circuits," *IEEE J. Solid-State Circuits*, vol. 29, pp. 655–662, June 1994.

[13] A. Kabbani and A. J. Al-Khalili, "Estimation of ground bounce effects on CMOS circuits," *IEEE Trans. Comp. Packag. Technol.*, vol. 22, pp. 316–325, June 1999.

[14] H. H. Chen and D. D. Ling, "Power supply noise analysis methodology for deep-submicron VLSI chip design," in *Proc. 1997 Design Automation Conf.*, Anaheim, CA, June 1997, pp. 638–643.

[15] Y. Eo, W. R. Eisenstadt, J. Y. Jeong, and O. K. Kwon, "A new on-chip interconnect crosstalk model and experimental verification for CMOS VLSI circuit design," *IEEE Trans. Electron Devices*, vol. 47, pp. 129–140, Jan. 2000.

[16] K. Joardar, "A simple approach to modeling cross-talk in integrated circuits," *IEEE J. Solid-State Circuits*, vol. 29, pp. 1212–1219, Oct. 1994.

[17] M. C. Johnson, D. Somasekhar, and K. Roy, "Models and algorithms for bounds on leakage in CMOS circuits," *IEEE Trans. Computer-Aided Design* , vol. 18, pp. 714–725, June 1999.

[18] S. Natarajan, M. A. Breuer, and S. K. Gupta, "Process variations and their impact on circuit operation," in *Proc. of Int. Symp. Defect and Fault Tolerance VLSI Syst.*, Austin, TX, Nov. 1998, pp. 73–81.

[19] T. R. N. Rao and E. Fujiwara, *Error-Control Coding for Computer Systems*. Englewood Cliffs, NJ: Prentice-Hall, 1989.

[20] G. R. Redinbo, "Generalized algorithm-based fault tolerance: Error correction via Kalman estimation," *IEEE Trans. Comput.*, vol. 47, pp. 639–655, June 1998.

[21] R. Karri, "Fault-tolerant VLSI systems," *IEEE Trans. Rel.*, vol. 48, pp. 106–107, June 1999.

[22] Y. Y. Chen, S. J. Upadhyaya, and C. H. Cheng, "A comprehensive reconfiguration scheme for fault-tolerant VLSI/WSI array processors," *IEEE Trans. Comput.*, vol. 46, pp. 1363–1371, Dec. 1997.

[23] C. Bolchini, G. Buonanno, D. Sciuto, and R. Stefanelli, "An improved fault tolerant architecture at CMOS level," in *Proc. Int. Symp. Circuits Syst.*, vol. 4, Hong Kong, June 1997, pp. 2737–2740.

[24] N. R. Shanbhag, "A mathematical basis for power-reduction in digital VLSI systems," *IEEE Trans. Circuits Syst. II*, vol. 44, pp. 935–951, Nov. 1997.

[25] R. Hedge and N. R. Shanbhag, "Toward achieving energy-efficiency in presence of deep submicron noise," *IEEE Trans. VLSI*, vol. 8, pp. 379–391, Aug. 2000.

[26] L. Wang and N. R. Shanbhag, "An energy-efficient, noise-tolerant dynamic circuit technique," *IEEE Trans. Circuits Syst. II*, vol. 47, pp. 1300–1306, Nov. 2000.

[27] R. Hegde and N. R. Shanbhag, "Soft digital signal processing," *IEEE Trans. VLSI Syst.*, vol. 9, pp. 813–823, Dec. 2001.

[28] R. Gonzalez, B. M. Gordon, and M. A. Horowitz, "Supply and threshold voltage scaling for low power CMOS," *IEEE J. Solid-State Circuits*, vol. 32, pp. 1210–1216, Aug. 1997.

[29] L. Wang and N. R. Shanbhag, "Low-power filtering via adaptive error-concellation," *IEEE Trans. Signal Process*, vol. 51, pp. 575–583, Feb. 2003.

[30] S. Haykin, *Adaptive Filter Theory*. Englewood Cliffs, NJ: Prentice-Hall, 1996.

[31] D. P. Bertsekas, *Nonlinear Programming*. Boston, MA: Athena Scientific, 1995.

[32] M. Goel and N. R. Shanbhag, "Dynamic algorithm transformations for low-power reconfigurable adaptive equalizer," *IEEE Trans. Signal Processing*, vol. 47, pp. 2821–2832, Oct. 1999.

[33] A. V. Oppenheim and R. W. Schafer, *Discrete-Time Signal Processing*. Englewood Cliffs, NJ: Prentice-Hall, 1994.

[34] G. Y. Wei and M. A. Horowitz, "A full digital, energy-efficient, adaptive power-supply regulator," *IEEE J. Solid-State Circuits*, vol. 34, pp. 520–528, Apr. 1999.

[35] S. Ramprasad, N. R. Shanbhag, and I. N. Hajj, "Decorrelating (DECOR) transformations for low-power digital filters," *IEEE Trans. Circuits Syst. II*, vol. 45, pp. 776–788, June 1999.

[36] N. Sankarayya, K. Roy, and D. Bhattacharya, "Algorithms for low power and high speed FIR filter realization using differential coefficients," *IEEE Trans. Circuits Syst. II*, vol. 44, pp. 488–497, June 1997.

[37] J. Kadambi, I. Crayford, and M. Kalkunte, *Gigabit Ethernet—Migrating to High Bandwidth LAN's*. Englewood Cliffs, NJ: Prentice-Hall, 1998.

[38] C. R. Baugh and B. A. Wooley, "A two's complement parallel array multiplication algorithm," *IEEE Trans. Comput.*, vol. C-22, pp. 1045–1047, Dec. 1973.

[39] M. G. Xakellis and F. N. Najm, "Statistical estimation of the switching activity in digital circuits," in *Proc. 31st Design Automation Conf.*, San Diego, CA, June 1994, pp. 728–733.

[40] S. Gupta and F. N. Najm, "Power modeling for high-level power estimation," *IEEE Trans. VLSI*, vol. 8, pp. 18–29, Feb. 2000.

Lei Wang (M'01) received the B.Engr. and M.Engr. degrees from Tsinghua University, Beijing, China, in 1992 and 1996, respectively, and the Ph.D. degree from the University of Illinois at Urbana-Champaign, in 2001. His Ph.D. research focus was on exploration of performance limits of deep submicron very large scale integration (VLSI) systems and development of noise-tolerance techniques for low-power signal processing and computing systems.

In Summer 1999, he was with Microprocessor Research Laboratory, Intel Corporation, Hillsboro, OR, where his work involved development of high-speed and noise-tolerant VLSI design techniques. In 2001, he joined Hewlett-Packard Microprocessor Technology Laboratories, Fort Collins, CO. His current research interests include design and implementation of low-power, high-speed and noise-tolerance VLSI systems.

Naresh R. Shanbhag (M'88–SM'98) received the B. Tech. degree from the Indian Institute of Technology, New Delhi, India, the M.S. degree from Wright State University, Dayton, OH, and the Ph.D. degree from the University of Minnesota, MN, all in electrical engineering, in 1988, 1990, and 1993, respectively.

From July 1993 to August 1995, he was with AT&T Bell Laboratories, Murray Hill, NJ, where he was responsible for the development of very large scale integration (VLSI) algorithms, architectures, and implementation of broadband data communications transceivers. In particular, he was the Lead-Chip Architect for AT&T's 51.84-Mb/s transceiver chips over twisted-pair wiring for asynchronous transfer mode (ATM)-LAN and broadband access chip-sets. Since August 1995, he has been with the Department of Electrical and Computer Engineering and the Coordinated Science Laboratory, University of Illinois-Urbana, where he is presently an Associate Professor and Director of the Illinois Center for Integrated Microsystems. At the University of Illinois, he founded the VLSI Information Processing Systems (ViPS) Group, whose charter is to explore issues related to low-power, high-performance, and reliable integrated circuit implementations of broad-band communications and digital signal processing systems spanning the algorithmic, architectural and circuit domains. He has published more than 90 journal articles, book chapters, and conference publications in this area and holds three U.S. patents. He is also a coauthor of the research monograph *Pipelined Adaptive Digital Filters* (Norwell, MA: Kluwer, 1994).

Dr. Shanbhag received the the 2001 IEEE TRANSACTIONS ON VERY LARGE SCALE INTEGRATION (VLSI) SYSTEMS Best Paper Award, the 1999 IEEE Leon K. Kirchmayer Best Paper Award, the 1999 Xerox Faculty Award, the National Science Foundation CAREER Award in 1996, and the 1994 Darlington Best Paper Award from the IEEE Circuits and Systems Society. From July 1997 through 2001, he was a Distinguished Lecturer for the IEEE Circuits and Systems Society. From 1997 to 1999, he served as an Associate Editor for the IEEE TRANSACTION ON CIRCUITS AND SYSTEMS—PART: II ANALOG AND DIGITAL SIGNAL PROCESSING. He has served on Technical Program Committees of various international conferences.